Dielectric relaxation and electronic structure of $BaAl_{1/2}Nb_{1/2}O_3$: x-ray photoemission and nuclear magnetic resonance studies

2008 J. Phys.: Condens. Matter 20 445206

(http://iopscience.iop.org/0953-8984/20/44/445206)

J. Phys.: Condens. Matter **20** (2008) 445206 (8pp) doi:10.1088/0953-8984/20/44/445206

Dielectric relaxation and electronic structure of $BaAl_{1/2}Nb_{1/2}O_3$: x-ray photoemission and nuclear magnetic resonance studies

Alo Dutta[1], T P Sinha[1], B Pahari[2], R Sarkar[2], K Ghoshray[2] and Santiranjan Shannigrahi[3]

[1] Department of Physics, Bose Institute, 93/1 Acharya Prafulla Chandra Road, Kolkata 700009, India
[2] ECMP Division, Saha Institute of Nuclear Physics, 1/AF Bidhannagar, Kolkata 700064, India
[3] Institute of Materials Research and Engineering (IMRE), 3 Research Link, 117602, Singapore

Received 18 March 2008, in final form 8 September 2008
Published 30 September 2008
Online at stacks.iop.org/JPhysCM/20/445206

Abstract

The frequency-dependent dielectric relaxation in barium–aluminium–niobate, $BaAl_{1/2}Nb_{1/2}O_3$ (BAN), at low temperatures (103–443 K) is investigated by alternating-current impedance spectroscopy in the framework of conductivity and electric modulus formalisms. The Havriliak–Negami expression is used to analyse the electric modulus data. The scaling behaviour of the imaginary part of the electric modulus suggests that the relaxation describes the same mechanism at various temperatures. The frequency-dependent conductivity spectra follow the power law. The electronic structure of BAN is studied using x-ray photoemission spectroscopy (XPS). The XPS data are analysed by the first-principles full potential linearized augmented-plane-wave method using density functional theory under the generalized gradient approximation. The electronic structure calculation reveals that the electrical properties of BAN are dominated by the interaction between niobium d-states and oxygen p-states. The ^{27}Al and ^{93}Nb nuclear magnetic resonance (NMR) studies of the sample are performed at 78 and 73 MHz, respectively, in the temperature range 4–295 K to understand the transport properties of charge carriers in terms of their dynamics on a microscopic level. The description of the NMR lineshape is given on the basis of analytical formulae. The NMR investigation confirms the chemical ordering of 1:1 Al/Nb in BAN.

1. Introduction

Complex perovskite oxides $[A(B'B'')O_3]$ with high values of permittivity have attracted much scientific attention due to their applications in microelectronics as capacitors and memory devices. High dielectric constants allow smaller capacitive components, thus offering the opportunity to decrease the size of the electronic devices [1].

Niobium-based oxides with complex perovskite-like structures are attractive candidates for use as dielectric resonators in wireless communication systems. In this context, the electronic structure [2, 3], dielectric [4, 5] and various other properties [6, 7] of calcium–aluminium–niobate, $CaAl_{1/2}Nb_{1/2}O_3$, and structural and dielectric properties of strontium–aluminium–niobate, $SrAl_{1/2}Nb_{1/2}O_3$ [8], have been investigated by various researchers. This has motivated us to study the electronic structure and dielectric properties of a similar system, barium–aluminium–niobate, $BaAl_{1/2}Nb_{1/2}O_3$ (BAN).

We have investigated the electronic structure of BAN by employing the full potential linearized augmented-plane-wave (FLAPW) method using density functional theory (DFT) under the generalized gradient approximation (GGA). The information associated with the spectral density function is accomplished by x-ray photoemission spectroscopy (XPS).

The observed XPS results are analysed with the calculated electronic structure data.

The low temperature dielectric relaxation of BAN is studied by alternating-current impedance spectroscopy (ACIS). ACIS is usually conducted by measuring small-signal impedance at different temperatures, sweeping the frequency over the required range. The investigation of the dielectric relaxation in BAN will provide an insight into the conduction mechanism.

The ^{27}Al and ^{93}Nb nuclear magnetic resonance (NMR) studies of BAN at 78 and 73 MHz, respectively, are performed in the temperature range 4–295 K to obtain detailed information about transport properties of charge carriers in terms of their dynamics on a microscopic level. The description of the NMR lineshape is given on the basis of analytical formulae to get the chemical ordering of Al/Nb in BAN.

2. Experiment

The solid state reaction technique was employed for the synthesis of BAN. Powders of reagent grade $BaCO_3$, Al_2O_3 and Nb_2O_5, taken in stoichiometric ratios, were mixed, calcined and finally sintered into a disc. A detailed preparation procedure and a high temperature dielectric study of the sample are given in a previous work [9]. The capacitance and the loss tangent $\tan\delta$ of the sample are measured in the temperature range from 103 to 443 K and in the frequency range from 50 Hz to 1 MHz by using a LCR meter (HIOKI). The temperature is controlled with a programmable oven. All the dielectric data are collected while heating at a rate of 0.5 °C min^{-1}. The complex dielectric modulus $M^\star(=1/\epsilon^\star)$, impedance $Z^\star(=M^\star/\mathrm{j}\omega C_o)$ and AC conductivity $\sigma(=\epsilon_o\epsilon''\omega)$ are obtained from the temperature dependence of the real (ϵ') and imaginary (ϵ'') components of the dielectric permittivity $\epsilon^\star(=\epsilon'-\mathrm{j}\epsilon'')$.

The XPS spectra are obtained using a photoelectron spectrometer (VG ESCALAB 2201-XL Imaging System, UK) with a monochromatized Al–Kα x-ray radiation source (1486.6 eV). The C 1s peak is used as the reference standard to determine the binding energy.

The ^{27}Al and ^{93}Nb NMR studies are performed at 78 and 73 MHz, respectively, in a Bruker MSL100 spectrometer with 7.04 T superconducting magnet. A home-built NMR probe with an rf coil made of silver is used to avoid spurious ^{63,65}Cu signals. The spectrum is recorded by applying a $\pi/2$–τ–$\pi/2$ solid echo sequence. Temperature variation studies in the range 4–295 K are performed in the Oxford continuous-flow He cryostat with an ITC503 temperature controller.

3. Experimental results and discussion

3.1. Dielectric spectroscopy

The dielectric relaxation of BAN can be analysed in terms of dipolar and conductivity relaxation mechanisms. For conductivity relaxation, the dispersion of the dielectric constant is determined by a locally inhomogeneous potential barrier with long-range charge-carrier diffusion [10], and the dielectric response can be described as a relationship between the electric modulus (M) and the impedance (Z). The relaxation time is determined by the reciprocal of the frequency where the maximum of the imaginary part of the electric modulus or impedance is centred. The peak height in Z against frequency plot is proportional to the resistance of the relaxation process while the peak height in M against frequency plot is inversely proportional to the capacitance.

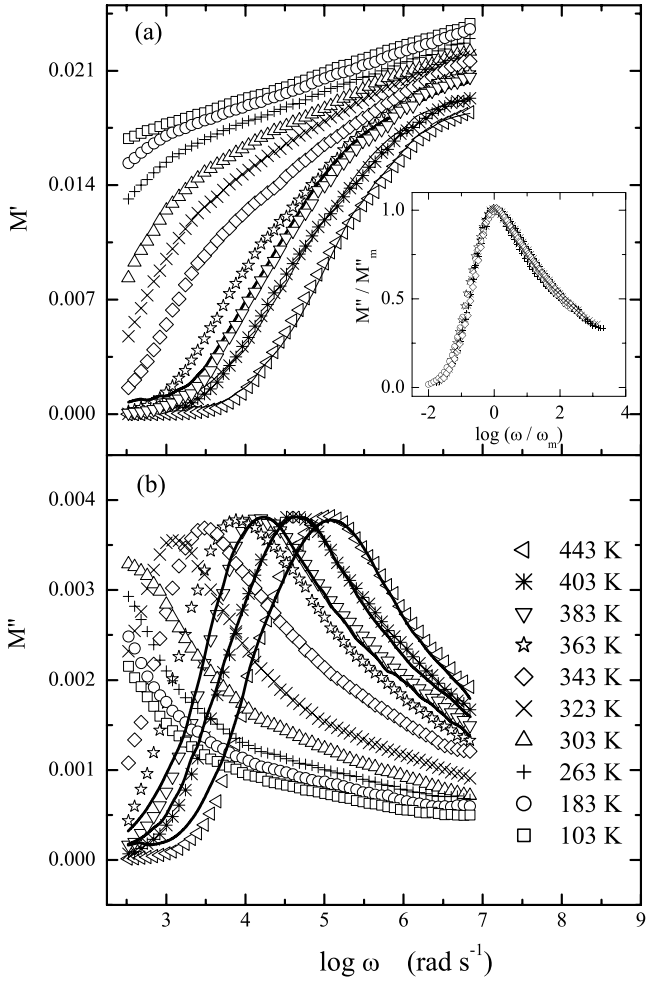

Figure 1. Frequency (angular) dependence of the M' (a) and M'' (b) of $BaAl_{1/2}Nb_{1/2}O_3$ at various temperatures. In the inset of (a), the scaling behaviour of M'' at various temperatures is shown.

Figure 1 displays the logarithmic frequency (angular) dependence of $M'(\omega)$ and $M''(\omega)$ for BAN at various temperatures. It can be seen that the values of M' increase with the increase of frequency and reach a constant value M_∞ (the asymptotic value of $M'(\omega)$ at higher frequencies (figure 1(a))). In the frequency range of this transition, peaks in the values of M'' are developed, indicating a relaxation process (figure 1(b)). The peak position shifts towards higher frequencies with an increase of temperature showing the thermally activated nature of the relaxation time. The frequency region below peak maximum (M''_{m}) determines the range in which charge carriers are mobile over long distances. At frequencies above peak maximum, the carriers are confined to potential wells, being mobile over short distances.

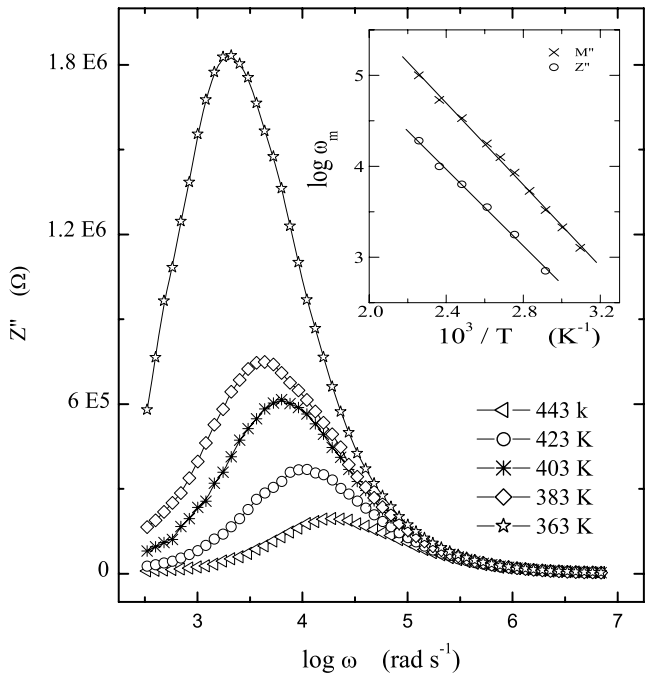

Figure 2. Frequency (angular) dependence of the Z'' of $BaAl_{1/2}Nb_{1/2}O_3$ at various temperatures. In the inset, the temperature dependence of the most probable relaxation frequency obtained from the frequency-dependent imaginary part of the impedance and electric modulus curves for $BaAl_{1/2}Nb_{1/2}O_3$ is shown where the symbols are the experimental points and the lines are the least-squares straight-line fit.

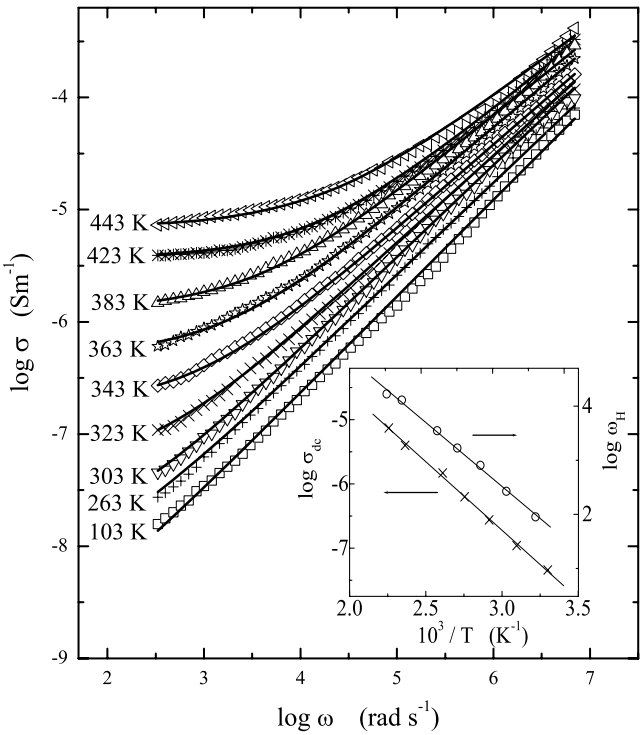

Figure 3. Frequency (angular) dependence of the conductivity (σ) of $BaAl_{1/2}Nb_{1/2}O_3$ at various temperatures. In the inset, temperature dependence of the dc conductivity and ω_H is shown where the symbols are the experimental points and the lines are the least-squares straight-line fit.

The dielectric relaxation in BAN can be modelled by the Debye [11], Cole–Cole [12, 13], Davidson–Cole [14] or Havriliak–Negami [15] equation. We have fitted our experimental data as shown by solid lines in figure 1 with the Havriliak–Negami expression defined as [16]

$$M' = \frac{M_\infty M_s[M_s A^\gamma + (M_\infty - M_s)\cos\gamma\phi]A^\gamma}{M_s^2 A^{2\gamma} + 2A^\gamma(M_\infty - M_s)M_s\cos\gamma\phi + (M_\infty - M_s)^2} \quad (1)$$

$$M'' = \frac{M_\infty M_s[(M_\infty - M_s)\sin\gamma\phi]A^\gamma}{M_s^2 A^{2\gamma} + 2A^\gamma(M_\infty - M_s)M_s\cos\gamma\phi + (M_\infty - M_s)^2} \quad (2)$$

where $A = [1 + 2(\omega\tau)^{1-\alpha}\sin(\alpha\pi/2) + (\omega\tau)^{2(1-\alpha)}]^{1/2}$ and $\phi = \tan^{-1}[(\omega\tau)^{1-\alpha}\cos(\alpha\pi/2)/1 + (\omega\tau)^{1-\alpha}\sin(\alpha\pi/2)]$; the values of α and γ lie in the range 0.018–0.022 and 0.39–0.45, respectively. Data presented in this way exhibit a pronounced relaxation peak for $M''(\omega)$ that moves towards lower frequencies during cooling of the sample. Consequently, it means that the relaxation rate for this process decreases with decreasing temperature. As a convenient measure of the characteristic relaxation time, one can choose the inverse of frequency of the maximum peak position, i.e. $\tau_m = \omega_m^{-1}$. Thus, we can determine the temperature dependence of the characteristic relaxation time as shown in the inset of figure 2, which satisfies the Arrhenius law. From the numerical fitting analysis, we have found the value of the activation energy = 0.44 eV.

We have scaled each M'' by M''_m (M''_m is the peak value of the imaginary part of the electric modulus) and each frequency by ω_m (ω_m corresponds to the frequency of the peak position of M'' in the M'' versus $\log\omega$ plots) in the inset of figure 1(a). The perfect overlap of the curves for all the temperatures into a single master curve indicates that the relaxation describes the same mechanism at various temperatures.

In figure 2, we have also plotted the logarithmic angular frequency dependence of the imaginary (Z'') part of the complex impedance of BAN at various temperatures. In the accessible frequency range, the spectrum of Z'' at each temperature exhibits one relaxation peak whose peak frequency, ω_m, increases with increasing temperature and follows the Arrhenius law with activation energy 0.42 eV, as shown in the inset of figure 2. Figure 2 indicates the spreading of the relaxation times. This would imply that the relaxation is temperature-dependent and there is apparently not a single relaxation time.

Figure 3 shows the log–log plot of frequency dependence of ac conductivity for BAN at various temperatures. The conductivity spectra display the typical shape found for an electronically conducting system. At higher temperatures, a plateau is observed in the plots in the low frequency region, i.e. a region where σ is frequency-independent. The plateau region extends to higher frequencies with increasing temperature. It is the region of dc conductivity, σ_{dc}. For higher frequencies, the conductivity increases with the increase of frequency. It is to be mentioned that, at low frequencies, random diffusion of charge carriers via hopping gives rise to a frequency-independent conductivity. At high frequencies,

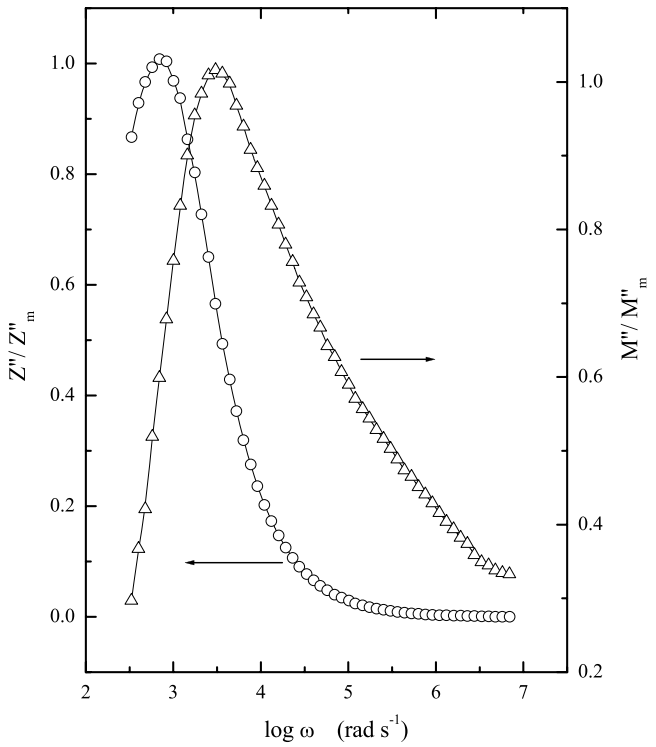

Figure 4. Frequency (angular) dependence of normalized peaks, $Z''/Z''_{\rm m}$ and $M''/M''_{\rm m}$, for $BaAl_{1/2}Nb_{1/2}O_3$ at 343 K.

$\sigma(\omega)$ exhibits dispersion, increasing in a power-law fashion and eventually becoming almost linear at higher frequencies. The real part of conductivity σ in such a situation can be expressed as [17]

$$\sigma = \sigma_{\rm dc}\left[1 + \left(\frac{\omega}{\omega_H}\right)^n\right] \tag{3}$$

where $\sigma_{\rm dc}$ is the dc conductivity, $\omega_{\rm H}$ is the hopping frequency of the charge carriers and n is the dimensionless frequency exponent. The experimental conductivity data are fitted to equation (3), where n is about 0.65 around 443 K and increases to a value of 0.86 around 103 K. The best fit of conductivity spectra is shown by solid lines in figure 3. The reciprocal temperature dependence of $\sigma_{\rm dc}$ and $\omega_{\rm H}$ as shown in the inset of figure 3 follows the Arrhenius law. The value of activation energy $E_{\rm H} = 0.44$ eV of the hopping frequency is close to the dc activation energy $E_\sigma = 0.43$ eV. Such a value of activation energy suggests that the primary charge transfer mechanism in the conduction process is small polaron hopping. It can be seen from figure 3 that, for BAN in the temperature range between 323 and 443 K, a frequency-independent conductivity ($\sigma_{\rm dc}$) appears due to the random hopping motion of the charge carriers giving a long-range conductivity effect. For the temperature below 323 K, the absence of dc conductivity in the accessible frequency range is due to a dipolar effect.

In figure 4, the variation of normalized parameters $M''/M''_{\rm m}$ and $Z''/Z''_{\rm m}$ as a function of logarithmic frequency measured at 343 K for BAN is shown. The position of the peak in the $Z''/Z''_{\rm m}$ is shifted to a lower frequency region in relation to the $M''/M''_{\rm m}$ peak. A comparison

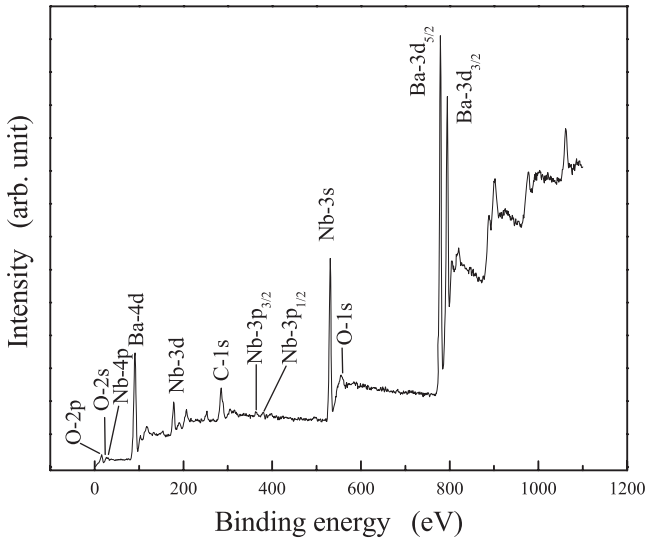

Figure 5. XPS spectrum of $BaAl_{1/2}Nb_{1/2}O_3$.

of the impedance with electric modulus data allows the determination of the bulk response in terms of localized or non-localized conduction [18]. The Debye model is related to an ideal frequency response of localized relaxation. The non-localized process known as the dc conductivity is dominated at low frequencies. The overlapping peak position of $M''/M''_{\rm m}$ and $Z''/Z''_{\rm m}$ curves is evidence of delocalized or long-range relaxation [18]. However, for the present system the $M''/M''_{\rm m}$ and $Z''/Z''_{\rm m}$ peaks do not overlap but are very close, suggesting the components from both long-range and localized relaxations.

3.2. Electronic structure and XPS study

We have calculated the electronic structure and hence the density of states (DOS) of BAN by using the first-principles FLAPW method [19] based on the GGA [20] within the framework of DFT [21, 22] in an undistorted Fm3m double perovskite structure. The volume corresponding to minimum energy (obtained from the volume optimization) gives the lattice parameter, $a = 2 \times 5.67$ Å. In our calculation, we have taken 47 k points in the first irreducible Brillouin zone and the density cutoff, i.e. $RK_{\rm max} = 7$. The self-consistency is achieved better than 0.0001 Ryd for energy density.

In order to verify the electronic structure calculations experimentally, we have performed the XPS study of BAN over a wide energy range. The obtained XPS spectrum is shown in figure 5. The profiles of the XPS spectrum are identified and indexed in figure 5. A spin–orbit doublet of Nb is obtained at 205.9 and 207.1 eV. Since the valence band is sensitive to the chemical surroundings, the XPS spectrum in the valence band energy region is very useful for the characterization of the chemical environment of elements. The valence band photoemission spectrum of BAN as shown in figure 6 shows a broad band centred at 15.9 eV with two shoulders at 12 and 8 eV. The valence band mainly consists of the oxygen p-states strongly hybridized with the niobium d-states. The shoulder at 8 eV comes from the non-bonding O-p states with

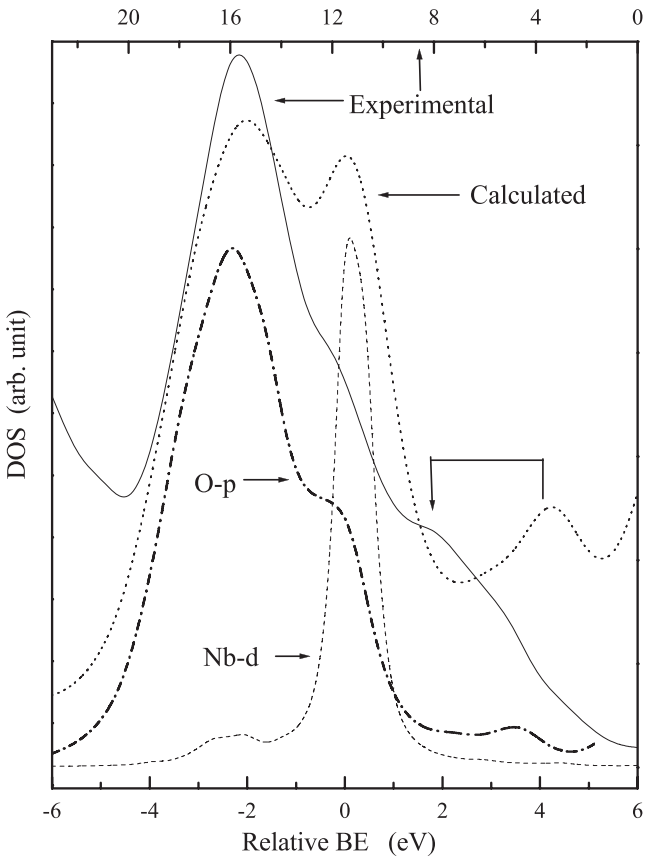

Figure 6. Experimental XPS spectrum (solid line) of $BaAl_{1/2}Nb_{1/2}O_3$ in valence band region is compared with the calculated one (dotted line). The dashed and dashed–dotted lines are the convoluted DOS spectra of Nb-d state and O-p state, respectively.

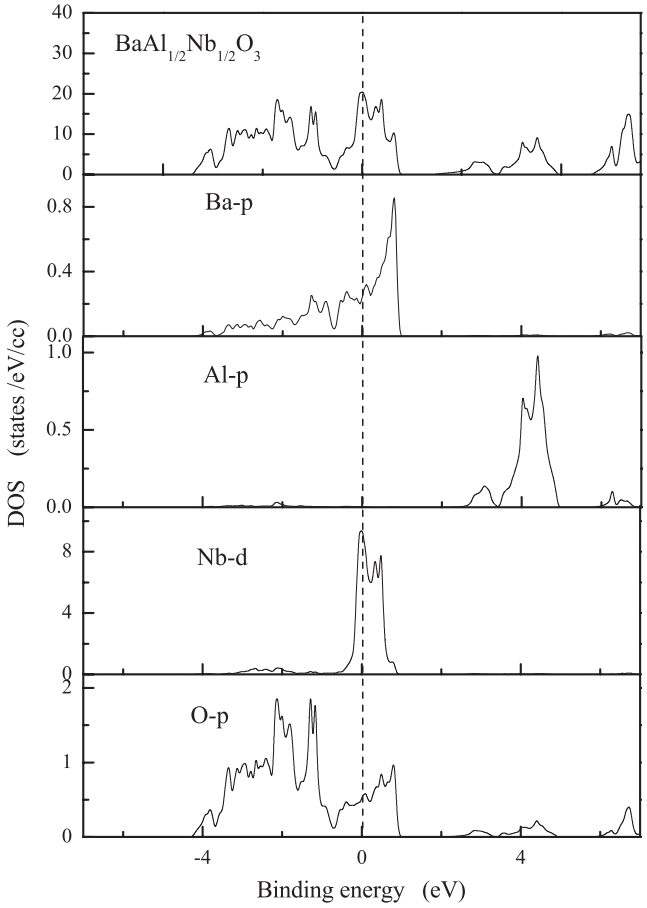

Figure 7. Total density of states and partial density of states of Ba-p, Al-p, Nb-d and O-p of $BaAl_{1/2}Nb_{1/2}O_3$.

minimal contribution from Nb-d states. These assignments will be further discussed.

Figure 7 shows the angular momentum decomposed total DOS of BAN with partial DOS of Ba-p, Al-p, Nb-d and O-p states. It is observed that the main contribution in the valence band comes from the O-p state with a small signature of the Ba-p state, while near the Fermi level (set at 0 eV), the contribution comes from the Nb-d state and O-p state. The basic critical ingredients in the DOS are the d-states of the Nb atom which in turn split into t_{2g} and e_g states by the crystal field produced by the oxygen octahedra, with the t_{2g} states having lower energy and the e_g states having higher energy.

The total DOS is convoluted with a Lorentzian of 0.5 eV full width at half-maximum and the calculated spectrum is compared with the experimental XPS valence band spectrum as shown in figure 6. The calculated electronic structure of BAN is qualitatively similar to that of the XPS spectrum in terms of spectral features, energy positions and relative intensities. To get more insight into the valence band spectrum near the Fermi level, we have also shown the convoluted angular momentum and site-decomposed partial DOS of Nb-d and O-p in figure 6. It is clear from the calculated total DOS and partial DOS of the O-p and Nb-d states that the broad peak at 15.9 eV arises from a bonding Nb(d)–O(p) interaction whereas the shoulder at 8 eV comes due to a non-bonding state of O-p. The shoulder appearing at 12 eV is contributed by the Nb-d states which are hybridized with O-p states. Since we have not included the lifetime broadening in the DOS calculation, the width of the calculated DOS curve gives sharper peaks than the experimental curve, causing a larger experimental bandwidth than the calculated one. This reduction of bandwidth is due to the muffin-tin approximation as observed by us in pure [23, 24] and complex [25] perovskites. The calculated spectra appear to be very similar to the peak positions of XPS spectra, thus implying a good agreement between the experimental results and our theoretical calculations.

The electronic structure calculation reveals that the electrical properties of BAN are dominated by the interaction between transition metal and oxygen ions. Its valence band consists mainly of the oxygen p-states hybridized with the niobium d-states. The e_g orbitals of the Nb cation overlap with the nearby $2p_\sigma$ orbital from the split O_{2p} to form σ-bonds (e_g–p_σ–e_g bond) and the t_{2g} orbitals overlap with $2p_\pi$ of O^{2-} ions to form weaker π-bonds (t_{2g}–p_π–t_{2g}) and may be responsible for the electrical properties.

As mentioned earlier, the XPS spectrum is very sensitive to the chemical environment of the elements, so the electronic structure calculation of BAN is fully based upon the chemical ordering of Al^{3+} and Nb^{5+} cations. The real existence of

chemical ordering of 1:1 Al/Nb in BAN is studied by a local method such as nuclear magnetic resonance.

3.3. ^{27}Al and ^{93}Nb NMR studies

In NMR experiments, the nuclei are sensitive to their local environment at a distance of less than 1 nm. The ^{27}Al and ^{93}Nb NMR studies are performed in a polycrystalline sample of BAN in the temperature range 4–295 K, in order to probe the local environments of the two different nuclear sites as a function of temperature. Figure 8 shows the ^{27}Al and ^{93}Nb NMR spectra at different experimental temperatures. It is seen that the ^{27}Al lines are almost symmetric over the whole temperature range; only the width and the spread of the lines towards the wings are enhanced with the lowering of temperature. Similar to ^{27}Al, the ^{93}Nb NMR lineshape also does not alter significantly up to 4 K, except for a small enhancement in the overall width of the resonance. As ^{27}Al ($I = 5/2$) and ^{93}Nb ($I = 9/2$) are both quadrupolar nuclei, they will interact with the electric field gradient (EFG) produced by the surrounding ions, creating a noncubic environment. So the resonance lineshape in this case will be governed by the chemical shift and the quadrupolar interaction. In order to determine both these parameters as a function of temperature, the experimental spectra are fitted theoretically using equation (4) [26]:

$$\begin{aligned}\nu(m \to m-1) = {} & \nu_R[1 + K_{iso} + K_{axial}(3\cos^2\theta - 1) \\ & + K_{aniso}\sin^2\theta\cos2\phi] + \frac{\nu_Q}{2}(m - 1/2)[(3\cos^2\theta - 1) \\ & + \eta\sin^2\theta\cos2\phi] + \left(\frac{\nu_Q^2}{32\nu_R}\right)(1 - \cos^2\theta)[(102m(m-1) \\ & - 18I(I+1) + 39)\cos^2\theta(1 + \tfrac{2}{3}\eta\cos2\phi) \\ & - (6m(m-1) - 2I(I+1) + 3)(1 - \tfrac{2}{3}\eta\cos2\phi)] \\ & + \left(\frac{\eta^2\nu_Q^2}{72\nu_R}\right)[24m(m-1) - 4I(I+1) \\ & + 9 - (30m(m-1) - 6I(I+1) + 12)\cos^2\theta \\ & - (\tfrac{51}{2}m(m-1) - \tfrac{9}{2}I(I+1) + \tfrac{39}{4})\cos^2 2\phi(\cos^2\theta - 1)^2] \end{aligned} \quad (4)$$

where

$$K_{iso} = \tfrac{1}{3}(K_1 + K_2 + K_3), \qquad K_{aniso} = \tfrac{1}{2}(K_2 - K_1),$$

$$K_{axial} = \tfrac{1}{6}(2K_3 - K_1 - K_2).$$

Here, K_1, K_2 and K_3 are the three principal values of the chemical shift tensor K. The polar and azimuthal angles, θ and ϕ, respectively, give the direction of the external magnetic field with respect to the eigenframe of K. ν_R, ν_Q and η are the resonance frequency of the probed nucleus in the absence of local electronic field in the solid, the quadrupolar splitting frequency and the asymmetry parameter, respectively.

In figure 9, the theoretical lines are shown over the experimental lines. In the case of Al, the resonance line can be well fitted considering a single line, i.e. only one type of Al site is present in the unit cell throughout the whole temperature range. This indicates that all the Al atoms in the unit cell are

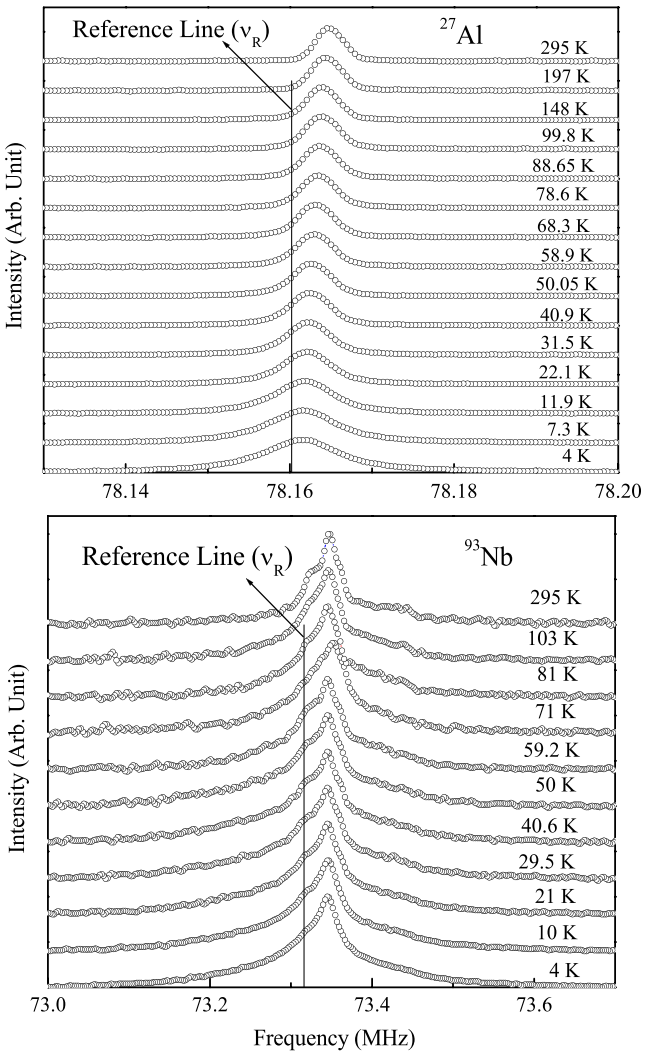

Figure 8. Experimental ^{27}Al and ^{93}Nb NMR spectra at various temperatures of $BaAl_{0.5}Nb_{0.5}O_3$.

in the same chemical environment and also experiencing the same EFG from the surrounding ions. Whereas in the case of Nb, it is seen that the experimental line can be well fitted only by considering it as a superposition of three constituent lines, namely lines 1, 2 and 3 with different hyperfine interaction parameters. Such a consideration is necessary throughout the whole temperature range as suggested by various researchers in Nb-based complex perovskite oxides [27–29]. The constituent lines are also shown in figure 9 together with the overall theoretical line. Lines 2 and 3 have comparatively smaller widths, indicating that the Nb atoms corresponding to these lines are situated in a more ordered arrangement of the surrounding atoms and hence experiencing less distribution of EFG.

Figures 10 and 11 show the temperature dependence of the hyperfine interaction parameters of ^{27}Al and ^{93}Nb nuclei, respectively. It is seen from figure 10 that ^{27}Al nuclei experience a very small positive isotropic shift (K_{iso}) at 295 K with zero anisotropy. The small value of K_{iso}, starts to decrease continuously from 100 K and continues till 4 K, whereas the anisotropic shift, which is almost zero in the

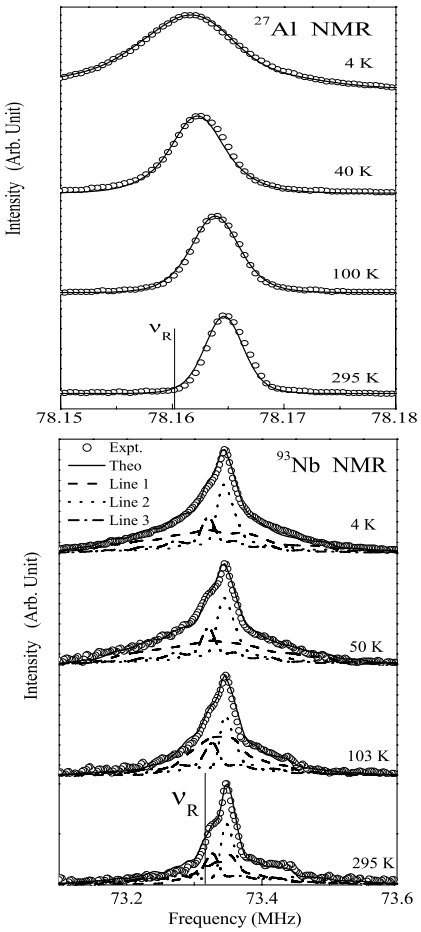

Figure 9. ^{27}Al and ^{93}Nb NMR spectra at some selected temperatures in $BaAl_{0.5}Nb_{0.5}O_3$. The solid lines represent the theoretical fittings by equations (4). In the case of Nb, the broken lines represent the three constituent lines required to fit the experimental data.

range 100–295 K, starts to increase continuously from around 50 K and continues till 4 K. Similar enhancement was also observed in the behaviour of ν_Q. Since the extent of the change in these parameters is not appreciably large, they may not indicate a long-range polar ordering near this temperature. However, it could be a signature of the beginning of the small asymmetric displacements of the surrounding atoms of the Al nuclei, resulting in an enhancement of electric field gradient and anisotropy in the chemical environment. Figure 11 shows the temperature dependence of the shift and quadrupolar interaction parameters for three constituent lines required to fit the experimental ^{93}Nb resonance. In this case, for lines 2 and 3 having negligible chemical shift anisotropy, all the chemical shift parameters together with the quadrupolar interaction parameters remain temperature-independent, suggesting no change in their chemical environment as well as the symmetry of the surrounding atoms. However, for site 1, with considerable chemical shift anisotropy, the temperature dependence of the shift parameters resembles that of the ^{27}Al resonance. The only difference is that the temperature dependence of ν_Q for this Nb line does not agree with that of the Al resonance which showed an enhancement below 100 K. Rather, it follows the same temperature-independent behaviour as shown by sites 2 and 3 of the Nb resonance.

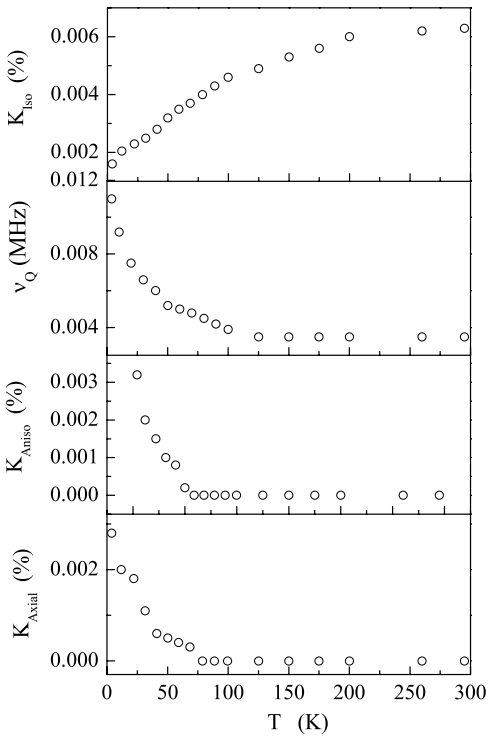

Figure 10. Temperature dependences of chemical shift and quadrupolar interaction parameters of ^{27}Al nucleus in $BaAl_{1/2}Nb_{1/2}O_3$.

4. Conclusions

The frequency-dependent dielectric relaxation of barium–aluminium–niobate, $BaAl_{1/2}Nb_{1/2}O_3$ (BAN) ceramic, synthesized by a solid state reaction technique is investigated in the temperature range from 103 to 443 K by alternating-current impedance spectroscopy. An analysis of the real and imaginary parts of the electric modulus is performed using the Havriliak–Negami expression. The activation energy calculated from frequency dependence of the imaginary part of the electric modulus is found to be $\simeq$0.44 eV, which suggests that the bulk conduction in BAN is due to small polaron hopping. The scaling behaviour of the imaginary part of the electric modulus (M'') suggests that the relaxation describes the same mechanism at various temperatures. The observed electrical data are also analysed in the framework of the conductivity formalism. The frequency-dependent conductivity spectra at various temperatures follow the power law. A comparison of the frequency-dependent spectra of the imaginary electric modulus with imaginary impedance suggests that both long-range and localized conduction are responsible for dielectric relaxation in BAN. The electronic structure of BAN is studied using x-ray photoemission spectroscopy (XPS). The total and partial density of states (DOS) of BAN are calculated by the first-principles full potential linearized augmented-plane-wave method using density functional theory under the generalized gradient approximation. The calculated DOS data are convoluted to explain the observed XPS spectra. The electronic structure calculation reveals that the electrical properties of BAN are dominated by the interaction between niobium and oxygen ions. The ^{27}Al and ^{93}Nb NMR studies

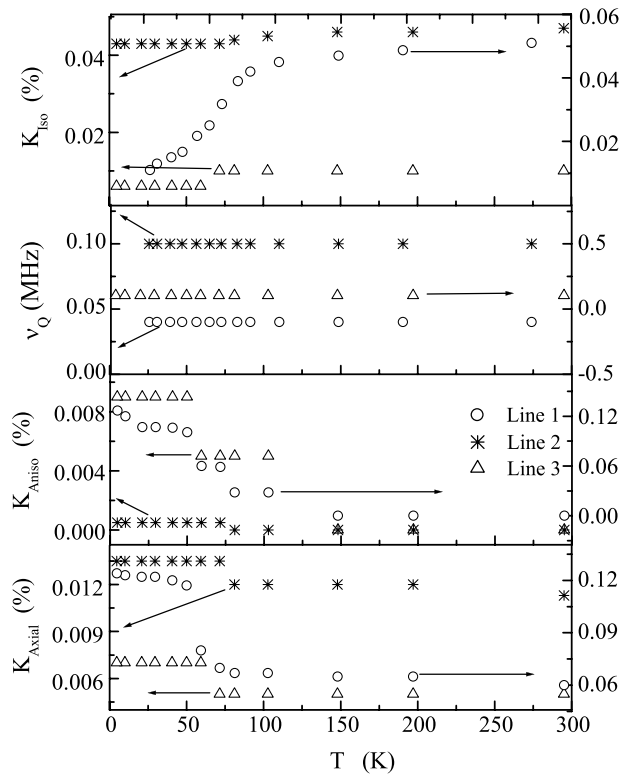

Figure 11. Temperature dependences of chemical shift and quadrupolar interaction parameters of ^{93}Nb nucleus in $BaAl_{1/2}Nb_{1/2}O_3$.

of BAN are performed at 78 and 73 MHz, respectively, in the temperature range 4–295 K to understand the transport properties of charge carriers in terms of their dynamics on a microscopic level. The description of the NMR lineshape is given on the basis of analytical formulae. From the present NMR investigations in a polycrystalline sample of BAN, it is revealed that local environments of all the Al atoms are almost identical at 295 K. However, the evolution of the spectral shape with temperature suggests an enhancement of the EFG and the chemical shift anisotropy parameter in the range 4–100 K, retaining the equivalency of all the Al sites. The same is not true for the Nb atoms, for which there are three types of sites in the temperature range 4–295 K. The local environment of only one type of Nb site is affected below 100 K, with the others remaining unaltered. The NMR study confirms the chemical ordering of 1:1 Al/Nb in BAN.

Acknowledgments

The authors thank Dr Eric Cockayne of the Ceramic Division, Materials Science and Engineering Laboratory, National Institute of Standards and Technology, Gaithersburg, MD for sending his data on $CaAl_{1/2}Nb_{1/2}O_3$ obtained by first-principles calculations.

References

[1] Cava R J 2001 *J. Mater. Chem.* **11** 54
[2] Cockayne E 2001 *J. Appl. Phys.* **90** 1459
[3] Cockayne E and Burton B P 2000 *Phys. Rev.* B **62** 3735
[4] Vanderah T A, Febo W, Chan J Y, Roth R S, Loezos J M, Rotter L D, Geyer R G and Minor D B 2000 *J. Solid State Chem.* **155** 78
[5] Kagata H and Kato J 1994 *Japan. J. Appl. Phys.* **33** 5463
[6] Levin I, Chan J Y, Maslar J E, Vanderah T A and Bell S M 2001 *J. Appl. Phys.* **90** 904
[7] Prosandeev S A, Waghmare U, Levin I and Maslar J 2005 *Phys. Rev.* B **71** 214307
[8] Chan J Y, Levin I, Vanderah T A, Geyer R G and Roth R S 2000 *Int. J. Inorg. Mater.* **2** 107
[9] Dutta A and Sinha T P 2006 *J. Phys. Chem. Solids* **67** 1484
[10] Macedo P B, Moynihan C T and Bose R 1972 *Phys. Chem. Glasses* **13** 171
[11] Debye P 1929 *Polar Molecules* (New York: Chemical Catalogue Company)
[12] Cole K S and Cole R H 1941 *J. Chem. Phys.* **9** 341
[13] Cole K S and Cole R H 1942 *J. Chem. Phys.* **10** 98
[14] Davidson D W and Cole R H 1951 *J. Chem. Phys.* **19** 1484
[15] Havriliak S and Negami S 1967 *Polymer* **8** 161
[16] Tsangaris G M, Psarras G C and Kouloumbi N 1998 *J. Mater. Sci.* **33** 2027
[17] Almond D P and West A R 1983 *Nature* **306** 456
[18] Gerhardt R 1994 *J. Phys. Chem. Solids* **55** 1491
[19] Blaha P, Schwarz K, Madsen G, Kvasnicka D and Luitz J 2001 *WIEN2k, An Augmented Plane Wave + Local Orbitals Program for Calculating Crystal Properties* Karlheinz Schwarz, Techn. Universität Wien, Austria ISBN3-9501031-1-2
[20] Perdew J P, Chevary J A, Vosko S H, Jackson K A, Pederson M R, Sing D J and Fiolhais C 1992 *Phys. Rev.* B **46** 6671
[21] Hohenberg P and Kohn W 1964 *Phys. Rev.* **136** B864
[22] Blaha P, Schwarz K, Sorantin P and Tricky S B 1990 *Comput. Phys. Commun.* **59** 399
[23] Saha S, Sinha T P and Mookerjee A 2000 *Phys. Rev.* B **62** 8828
[24] Saha S, Sinha T P and Mookerjee A 2000 *J. Phys.: Condens. Matter* **12** 3325
[25] Dutta A, Sinha T P and Shannigrahi S 2007 *Phys. Rev.* B **76** 155113
[26] Baugher J F, Taylor P C, Oja T and Bray P J 1968 *J. Chem. Phys.* **50** 4914
[27] Laguta V V, Glinchuk M D, Bykov I P, Blinc R and Zalar B 2004 *Phys. Rev.* B **69** 054103
[28] Blinc R, Gregorovic A, Zalar B, Pirc R, Laguta V V and Glinchuk M D 2001 *J. Appl. Phys.* **89** 1349
[29] Laguta V V, Glinchuk M D, Nokhrin S N, Bykov I P, Blinc R, Gregorovic A and Zalar B 2003 *Phys. Rev.* B **67** 104106